

Article

# Fabrication of Low Dislocation Density, Single-Crystalline Diamond via Two-Step Epitaxial Lateral Overgrowth

Fengnan Li, Jingwen Zhang, Xiaoliang Wang, Minghui Zhang and Hongxing Wang \*

Key Laboratory for Physical Electronics and Devices of the Ministry of Education, Xi'an Jiaotong University, Xi'an 710049, China; lfn@stu.xjtu.edu.cn (F.L.); jwzhang@mail.xjtu.edu.cn (J.Z.); xlwang@semi.ac.cn (X.W.); zhangminghuicc@mail.xjtu.edu.cn (M.Z.)

\* Correspondence: hxwangcn@mail.xjtu.edu.cn; Tel.: +86-29-8266-8155

Academic Editor: Yuri N. Palyanov

Received: 15 March 2017; Accepted: 17 April 2017; Published: 18 April 2017

**Abstract:** Continuous diamond films with low dislocation density were obtained by two-step epitaxial lateral overgrowth (ELO). Grooves were fabricated by inductively coupled plasma etching. Mo/Pd stripes sputtered in the grooves were used to inhibit the propagation of dislocations originating from the diamond substrate. Coalescent diamond films were achieved by ELO via microwave plasma-enhanced chemical vapor deposition. Etch-pits were formed intentionally to characterize the quality of the epitaxial films and distinguish different growth areas, as dislocations served as preferential sites for etching. In the window regions, a high density of dislocations, displayed as dense etch-pits, was generated. By contrast, the etch-pit density was clearly lower in the overgrowth regions. After the second ELO step, the dislocation density was further decreased. Raman spectroscopy analysis suggested that the lateral overgrowth of diamond is a promising method for achieving low dislocation density films.

**Keywords:** chemical vapor deposition; CVD diamond; epitaxial lateral overgrowth (ELO); dislocations; etch-pits

## 1. Introduction

Diamond exhibits attractive intrinsic properties, such as a wide band gap energy (5.47 eV), high electric breakdown field (10 MV·cm<sup>-1</sup>), high carrier mobility (3800 cm<sup>2</sup>·V<sup>-1</sup>·s<sup>-1</sup> for holes), high thermal conductivity (22 W·cm<sup>-1</sup>), and low dielectric constant (~5.7), making it a promising material for future electronic devices [1–5]. However, extended defects, such as dislocations and stacking faults, are common in both natural and synthetic diamond. For crystals formed via chemical vapor deposition (CVD), dislocations mainly stem from extended defects related to the substrate, such as defects in the substrate surface and defects in the bulk of the substrate. Dislocations tend to thread through the CVD film almost parallel to the growth direction [6]. Epitaxial lateral overgrowth (ELO) is a useful method to suppress the dislocation density and has been used for the growth of GaN [7–10]. The ELO method has also been applied to the growth of diamond [11,12].

Although X-ray topography, cathodoluminescence and transmission electron microscopy can be used to observe and quantify dislocations in diamond, these methods are relatively difficult to apply since they require complicated sample preparation or heavy equipment [13–15]. Moreover, it is very difficult to distinguish areas of different growth quality for the purpose of fabricating a metal mask by the ELO process, since the differences can be seen only under the observation of heavy equipment. Since lattice defects, such as vacancies, dislocations, and impurities, serve as preferential sites for etching, plasma etching treatment can be used to characterize and distinguish different growth areas

by dislocation density [6]. As etch-pits are formed after plasma etching treatment, it is quite convenient to assess the growth quality in different areas. In addition, the etch-pits, which can be observed under optical microscopy, can be used as markers for pattern alignment in the subsequent ELO process.

In this work, two-step ELO via microwave plasma-enhanced chemical vapor deposition (MPCVD) was used to fabricate low dislocation density, single-crystalline diamond. Grooves were fabricated by inductively coupled plasma etching. Mo/Pd stripes sputtered in the grooves were used to hinder the propagation of dislocations originating from the diamond substrate. Plasma etching was used to characterize the quality of the epitaxial films and distinguish the different growth areas. Finally, the ELO diamond was also characterized by Raman spectroscopy and field emission scanning electron microscopy (FE-SEM).

## 2. Results and Discussion

Figure 1 shows the schematic process diagram of the ELO method. From Step 1 to Step 2, an Al mask with 1- $\mu\text{m}$ -thick stripes was patterned on the high-temperature high-pressure (HPHT) diamond substrate. The width of the Al stripes and spacing were 10 and 40  $\mu\text{m}$ , respectively. Grooves with a depth of 2  $\mu\text{m}$  were fabricated in the area without Al stripe coverage via inductively coupled plasma (ICP) etching. During the ICP etching process, the Al stripes protected the underlying diamond from etching. After ICP etching, the thickness of the Al stripes decreased to approximately 200 nm.

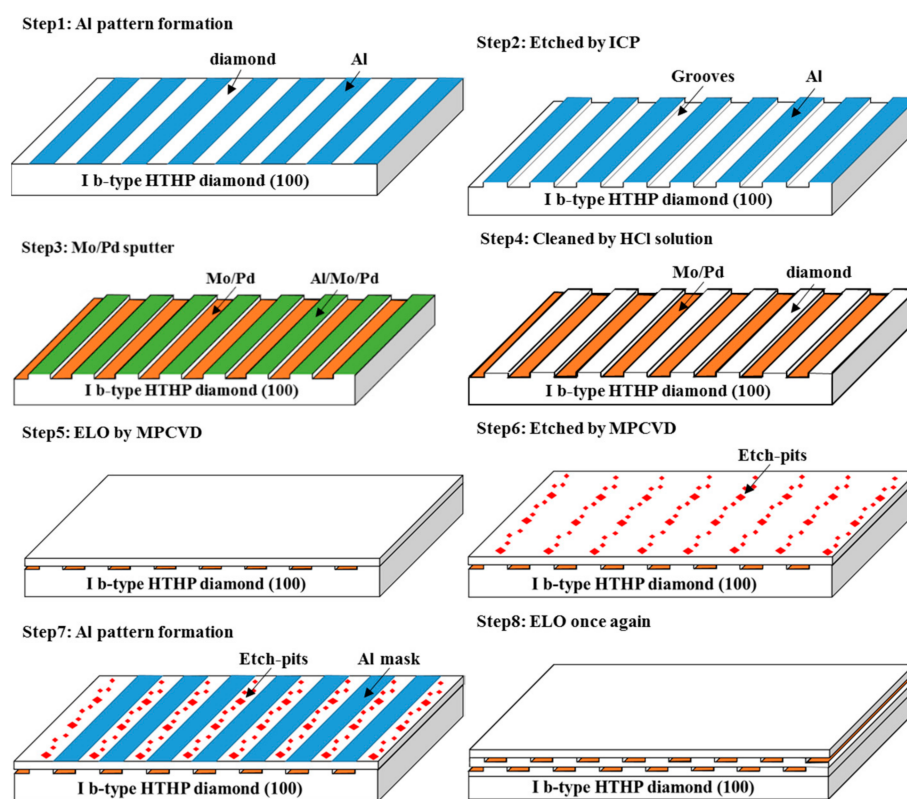


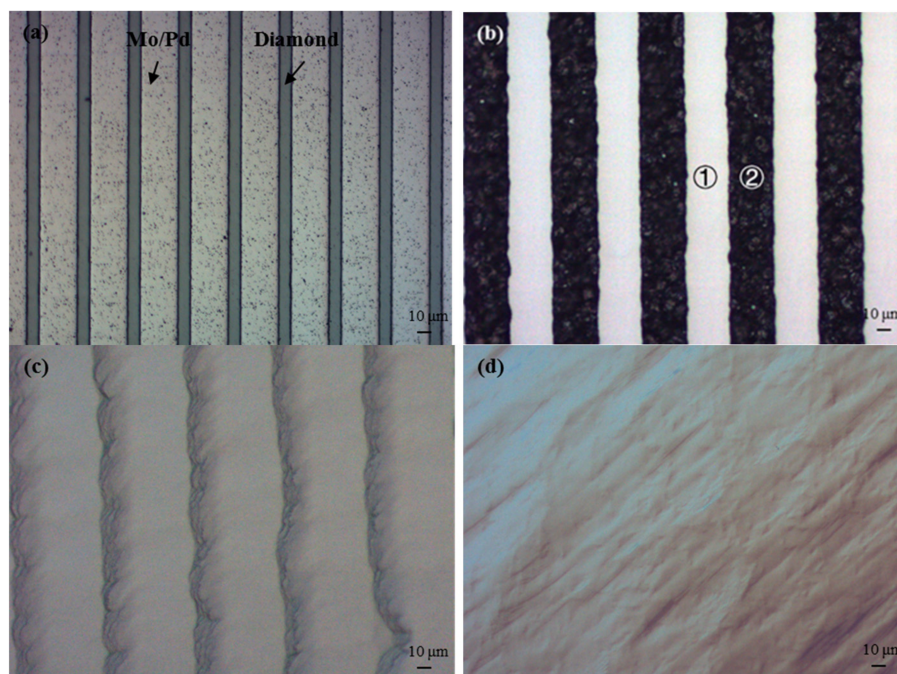
**Figure 1.** The schematic process diagram of the two-step epitaxial lateral overgrowth (ELO) method.

From Step 3 to Step 4, 100 nm Mo and 50 nm Pd layers were sputtered on the sample surface. The Mo layer was used to enhance the adhesion with the diamond surface, and the Pd layer was used to suppress the vertical growth of diamond. After metal sputtering, the sample was ultrasonically cleaned with an HCl solution. During this process, the Al stripes were able to lift-off the Mo/Pd layers. Thus, the areas covered with Al/Mo/Pd layers were cleaned to expose diamond windows. However, the area in the grooves covered with Mo/Pd layers were preserved after cleaning with HCl solution.

From Step 5 to Step 6, a diamond film with a thickness of 200  $\mu\text{m}$  was grown by MPCVD, which produced a continuous and flat surface by lateral overgrowth. Then, the surface of the ELO layer was treated by plasma etching to form etch-pits. The stripes with high etch-pit density were grown by conventional homoepitaxial growth, and the stripes with low etch-pit density were grown by lateral overgrowth. After the first ELO step, half of the diamond surface improved in quality.

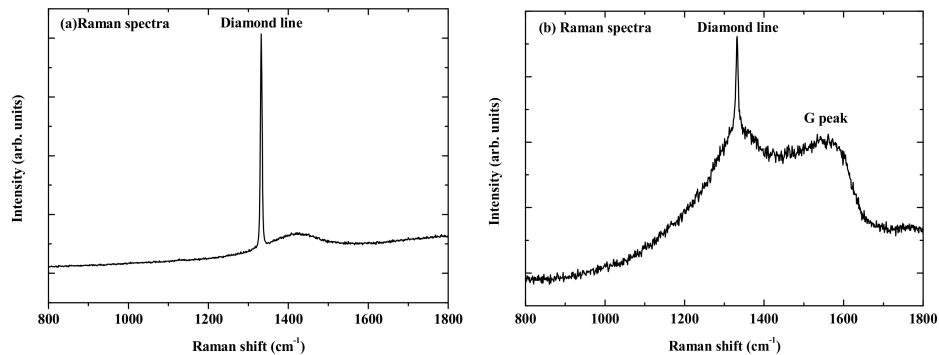
From Step 7 to Step 8, the above process was performed again for the second ELO step. During the process, the half of the diamond surface with high etch-pit density improved in quality via ELO. Since etch-pits can be observed under optical microscopy, they were used as markers for pattern alignment in the second ELO process. It should be mentioned that the Al stripes were fabricated on the lateral overgrowth area that did not show a distribution of etch-pits, thus forming diamond windows in this area during the second ELO step, as this area had a relatively lower dislocation density. Finally, the quality of the whole epitaxial film was improved.

Figure 2 shows optical images taken during the first ELO step. Figure 2a shows the image of the substrate after ultrasonic cleaning with an HCl solution. The grooves are covered with Mo/Pd layers, and the remaining areas are diamond windows. Figure 2b shows an image of the sample after 40 min of MPCVD growth. It can be observed that the diamond windows broadened from 10  $\mu\text{m}$  to 25  $\mu\text{m}$  by lateral overgrowth, as indicated in Area ①. Meanwhile, amorphous carbon formed on the Mo/Pd layers in the grooves, as indicated in Area ②. Figure 2c shows an image of the sample after 80 min of MPCVD growth. It can be observed that the diamond windows connected to form a continuous film. As the lateral overgrowth rate of diamond is much higher than the rate of amorphous carbon formation, the amorphous carbon was completely covered by diamond. However, the surface of the diamond film is not flat but instead has obvious stripes. Figure 2d shows the image of the sample after 240 min of MPCVD growth. It can be observed that the surface of the diamond film became smooth and flat.



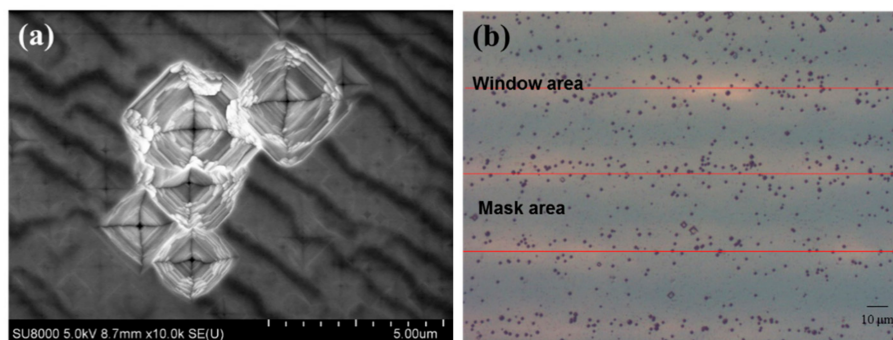
**Figure 2.** Optical images during the first ELO step. Panel (a) shows an image of the sample before MPCVD growth. Panels (b–d) show optical images of the sample after microwave plasma-enhanced chemical vapor deposition (MPCVD) growth for 40, 80 and 240 min, respectively. In Panel (b), Area ① and Area ② were originally diamond windows and Mo/Pd layers in the grooves, respectively.

Figure 3a,b show the Raman spectra obtained from two different areas, ① and ②, as indicated in Figure 2b. The Raman excitation wavelength was 532 nm. For Area ②, both the first-order diamond Raman line (located at  $1332\text{ cm}^{-1}$ ) and the  $\text{sp}^2$  amorphous carbon peak (located at  $1520\text{--}1580\text{ cm}^{-1}$ ) can be observed. This suggests that amorphous carbon was first formed on the Mo/Pd stripes. In the spectrum of Area ①, the  $\text{sp}^2$  amorphous carbon peak is no longer observed. Meanwhile, the full width at half maximum (FWHM) of the diamond Raman line is much smaller. A peak located at  $1430\text{--}1470\text{ cm}^{-1}$  appears in the Raman spectrum, which is related to the photoluminescence of CVD diamond.



**Figure 3.** (a) Raman spectra obtained from area ① in Figure 2b. (b) Raman spectra obtained from area ② in Figure 2b.

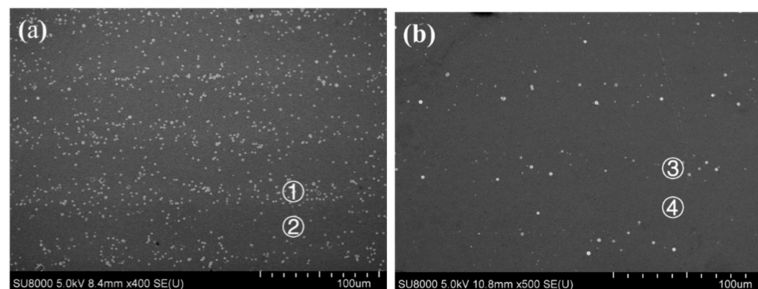
Figure 4 shows images of the surface of the first ELO layer after plasma etching by MPCVD for 15 min.  $\text{H}_2/\text{O}_2$  plasma etching treatments under relatively high pressure/power ( $>100\text{ mbar}$ ,  $>2000\text{ W}$ ) and with a low amount of added oxygen ( $<4\%$ ), usually lead to very selective etching of the (100) diamond surface [6]. Thus, defects such as dislocations located near the diamond surface typically appear as inverted pyramids with a square base after selective plasma etching. The structure of the inverted pyramids can be clearly observed in Figure 4a. The backlit optical image in Figure 4b shows that the etch-pits were concentrated in lines. Moreover, the etch-pit lines were located in the bright area. Since the window areas are transparent and the mask area blocks the backlight, this observation suggests that the lateral growth area had a low dislocation density.



**Figure 4.** (a) FE-SEM image of etch-pits formed by plasma etching for 15 min. (b) Backlit optical image of the first ELO layer after plasma etching for 15 min.

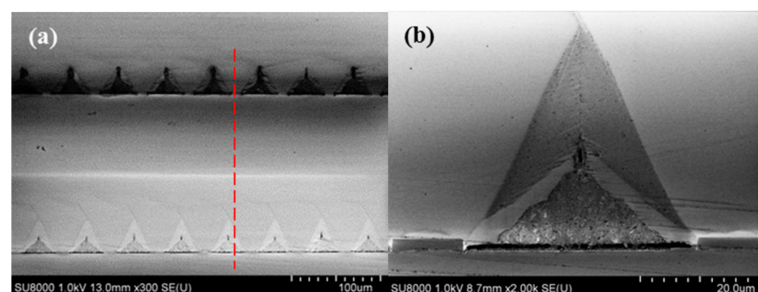
Figure 5 shows FE-SEM images of the first and second ELO layer after plasma etching for 15 min. As seen in Figure 5a, the etch-pits are distributed in stripes on the surface of the first ELO layer. Dislocations originating from the substrate windows propagate to the surface, which cause dense etch-pit formation upon plasma etching. By contrast, the dislocations were effectively blocked from

propagating in the lateral overgrowth area. Thus, the etch-pit density was clearly lower in these areas. As seen in Figure 5b, the etch-pits distributed in the stripes can still be observed on the surface of the second ELO layer, but the density clearly decreased. Because the dislocation density on the diamond windows decreased, fewer dislocations propagated to the surface to form etch-pits after the second ELO step. Thus, after two steps of ELO, the quality of the CVD diamond film was improved by reducing the dislocation density.



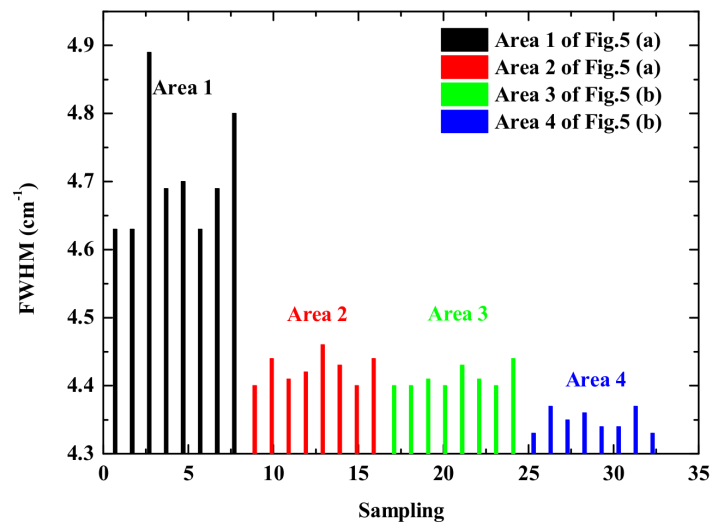
**Figure 5.** (a) FE-SEM image of the first ELO layer after plasma etching for 15 min. (b) FE-SEM image of the second ELO layer after plasma etching for 15 min.

Figure 6 shows FE-SEM images of the cross section of the sample after two steps of ELO. In the second ELO step, the diamond windows were located on top of the Mo/Pd stripes, leading to low dislocation density, as indicated by the dashed line. As seen in Figure 6, dark-colored triangular areas appear on the Mo/Pd stripes, which are related to amorphous carbon. A small hole and a vertical borderline can be clearly observed, which are formed when the two growth fronts of diamond coalesce. The results are in accordance with Figure 2. Initially, amorphous carbon formed on the Mo/Pd layers in the grooves. Then, the diamond windows were connected to form a continuous film by ELO.



**Figure 6.** FE-SEM images of the cross section of the sample after two steps of ELO. Panel (a) shows an image of the cross section with two ELO layers. Panel (b) shows an image of the coalescent area.

Figure 7 shows the FWHMs of the diamond Raman lines obtained from the different surface areas after ELO, as indicated in Figure 5a,b. After the first ELO step, the FWHMs obtained from dense etch-pit Area ① ranged from  $4.62$  to  $4.89$   $\text{cm}^{-1}$ . By contrast, the FWHMs obtained from the sparse etch-pit Area ② were all approximately  $4.42$   $\text{cm}^{-1}$ . This indicates that the crystalline structure of the lateral overgrowth area was improved. After the second ELO step, the FWHMs obtained from the dense etch-pit Area ③ were all still approximately  $4.42$   $\text{cm}^{-1}$ . This indicates that dislocations propagated to the surface. However, the FWHMs obtained from the sparse etch-pit Area ④ decreased to approximately  $4.35$   $\text{cm}^{-1}$ . This suggests that the crystalline structure was further improved after the second ELO step.



**Figure 7.** Full width at half maximum values (FWHMs) of the diamond Raman lines obtained from the different areas indicated in Figure 5.

### 3. Materials and Methods

An Ib-type high-temperature high-pressure (HPHT) diamond (100) substrate ( $3 \times 3 \times 0.5 \text{ mm}^3$ ) was used in this experiment. Before epitaxial layer growth, the substrate was cleaned in a mixed solution of nitric and sulfuric acids at  $250 \text{ }^\circ\text{C}$  for 1 h. The growth conditions were as follows: substrate temperature:  $\sim 1150 \text{ }^\circ\text{C}$ ;  $\text{H}_2$  flow:  $\sim 500 \text{ sccm}$ ;  $\text{CH}_4$  flow:  $\sim 50 \text{ sccm}$ ; gas pressure:  $\sim 120 \text{ Torr}$ . The etch-pit formation conditions were as follows: substrate temperature:  $\sim 1020 \text{ }^\circ\text{C}$ ;  $\text{H}_2$  flow:  $\sim 400 \text{ sccm}$ ;  $\text{O}_2$  flow:  $\sim 8 \text{ sccm}$ ; gas pressure:  $\sim 120 \text{ Torr}$ . The ICP etching conditions were as follows: power:  $800 \text{ W}$ ; Ar flow:  $\sim 20 \text{ sccm}$ ;  $\text{O}_2$  flow:  $\sim 40 \text{ sccm}$ ; gas pressure:  $\sim 10 \text{ mTorr}$ .

### 4. Conclusions

Two-step ELO on an HPHT diamond (100) substrate by MPCVD was used to fabricate a low dislocation density, single-crystalline diamond. Grooves were fabricated by ICP etching on the diamond surface, followed by sputtering Mo/Pd stripes in the grooves. Metal stripes were used to inhibit the propagation of dislocations originating from the diamond substrate by suppressing the vertical growth of diamond on the metal stripes. Plasma etching was used to characterize the quality of the epitaxial films and distinguish different growth areas.

After the first ELO step, the FE-SEM images show that the etch-pit density was clearly lower in the lateral overgrowth area. Then, the etch-pits, which can be observed under optical microscopy, were used as markers for pattern alignment in the second ELO process. Grooves and Mo/Pd stripes were fabricated again on the areas with a high density of etch-pits. After the second ELO step, the FE-SEM images show that the etch-pit density further decreased in the lateral overgrowth area. Thus, the quality of the whole epitaxial film was improved.

**Acknowledgments:** This work was supported by the Ministry of Science and Technology (Grant No. 2013AA03A101) of China.

**Author Contributions:** Fengnan Li designed and carried out the experiments. Jingwen Zhang and Xiaoliang Wang grew and etched the diamond films. Minghui Zhang and Hongxing Wang analyzed the results and reviewed the manuscript.

**Conflicts of Interest:** The authors declare no conflict of interest.

## References

1. May, P.W. The new diamond age. *Science* **2008**, *320*, 1490–1491.
2. Isberg, J.; Hammersberg, J.; Johansson, E.; Wikstrom, T.; Twitchen, D.J.; Whitehead, A.J.; Coe, S.E.; Scarsbrook, G.A. High carrier mobility in single-crystal plasma-deposited diamond. *Science* **2002**, *297*, 1670–1672. [[CrossRef](#)] [[PubMed](#)]
3. Isberg, J.; Hammersberg, J.; Twitchen, D.J.; Whitehead, A.J. Single crystal diamond for electronic applications. *Diam. Relat. Mater.* **2004**, *13*, 320–324. [[CrossRef](#)]
4. Liao, M.Y.; Koide, Y. High-performance metal-semiconductor-metal deep-ultraviolet photodetectors based on homoepitaxial diamond thin film. *Appl. Phys. Lett.* **2006**, *89*, 113509. [[CrossRef](#)]
5. Liu, J.W.; Liao, M.Y.; Imura, M.; Tanaka, A.; Iwai, H.; Koide, Y. Low on-resistance diamond field effect transistor with high-k ZrO<sub>2</sub> as dielectric. *Sci. Rep.* **2014**, *4*, 06395. [[CrossRef](#)] [[PubMed](#)]
6. Naamoun, M.; Tallaire, A.; Silva, F.; Achard, J.; Doppelt, P.; Gicquel, A. Etch-pit formation mechanism induced on HPHT and CVD diamond single crystals by H<sub>2</sub>/O<sub>2</sub> plasma etching treatment. *Phys. Status Solidi A* **2012**, *209*, 1715–1720. [[CrossRef](#)]
7. Nam, O.H.; Bremser, M.D.; Zheleva, T.S.; Davis, R.F. Lateral epitaxy of low defect density GaN layers via organometallic vapor phase epitaxy. *Appl. Phys. Lett.* **1997**, *71*, 2638–2640. [[CrossRef](#)]
8. Sakai, A.; Sunakawa, H.; Usui, A. Defect structure in selectively grown GaN films with low threading dislocation density. *Appl. Phys. Lett.* **1997**, *71*, 2259–2261. [[CrossRef](#)]
9. Beaumont, B.; Bousquet, V.; Vennegues, P.; Vaille, M.; Bouille, A.; Gibart, P.; Dassonneville, S.; Amokrane, A.; Sieber, B. A two-step method for epitaxial lateral overgrowth of GaN. *Phys. Status Solidi A* **1999**, *176*, 567–571. [[CrossRef](#)]
10. Hiramatsu, K.; Nishiyama, K.; Onishi, M.; Mizutani, H.; Narukawa, M.; Motogaito, A.; Miyake, H.; Iyechika, Y.; Maeda, T. Fabrication and characterization of low defect density GaN using facet-controlled epitaxial lateral overgrowth (FACELO). *J. Cryst. Growth* **2000**, *221*, 316–326. [[CrossRef](#)]
11. Bauer, T.; Schreck, M.; Stritzker, B. Epitaxial lateral overgrowth (ELO) of homoepitaxial diamond through an iridium mesh. *Diam. Relat. Mater.* **2007**, *16*, 711. [[CrossRef](#)]
12. Ando, Y.; Kamano, T.; Suzuki, K.; Sawabe, A. Epitaxial Lateral Overgrowth of Diamonds on Iridium by Patterned Nucleation and Growth Method. *Jpn. J. Appl. Phys.* **2012**, *51*, 090101. [[CrossRef](#)]
13. Kono, S.; Teraji, T.; Kodama, H.; Sawabe, A. Imaging of diamond defect sites by electron-beam-induced current. *Diam. Relat. Mater.* **2015**, *59*, 54–61. [[CrossRef](#)]
14. Umezawa, H.; Kato, Y.; Watanabe, H.; Omer, A.M.M.; Yamaguchi, H.; Shikata, S. Characterization of crystallographic defects in homoepitaxial diamond films by synchrotron X-ray topography and cathodoluminescence. *Diam. Relat. Mater.* **2011**, *20*, 523–526. [[CrossRef](#)]
15. Gaukroger, M.P.; Martineau, P.M.; Crowder, M.J.; Friel, I.; Williams, S.D.; Twitchen, D.J. X-ray topography studies of dislocations in single crystal CVD diamond. *Diam. Relat. Mater.* **2008**, *17*, 262–269. [[CrossRef](#)]

